# Site Specific Issues on Strong Ground Motion during the Kocaeli, Turkey Earthquake of August 17, 1999, as Inferred from Array Observations of Microtremors and Aftershocks

**by**

**Kazuyoshi Kudo, Tatsuo Kanno, Hiroshi Okada, Oguz Özel, Mustafa Erdik, Masayoshi Takahashi, Tsutomu Sasatani, Sadanori Higashi, and Kunikazu Yoshida**

ABSTRACT Array observations of microtremors and aftershocks were carried out near permanent strong motion observation sites run by Kandilli Observatory & Earthquake Research Institute as well as Ministry of Public Works and Settlement and damaged areas after the Kocaeli, Turkey earthquake of August 17, 1999. Major objectives are to determine S-wave velocity structures and to understand the site effects relatively on strong motion or damage. Most strong motion sites near the fault are classified to stiff and/or very hard soil. The records cannot directly be used for interpreting damage of buildings in sedimentary basin.

A large and long duration of strong motion records at ATS, near Avcilar, west of Istanbul are closely related to the low velocity (Vs~200 m/sec) of surface layers. The S-wave velocity structure at Avcilar where severely damaged during the mainshock is similar to the lowland (ATS) and it differs significantly from that of CNA where the strong motion record from the mainshock was obtained and it locates 4 km northeast from Avcilar. The strong ground motion at Avcilar during the mainshock is estimated to be similar to that at ATS. The strong motion sites, Sakarya (SKR) is located on very hard soil, while thick and soft sediments covers downtown Adapazari. It is plausible that strong ground motions during the mainshock at damaged area, ADC, were significantly different from those of SKR. A large difference of strong motions between a hillside and Izmit Bay area in and around Golcuk is also indicated by the comparison of aftershock records.

# Introduction

The major damage of buildings and loss of lives during the Kocaeli (Izmit), Turkey earthquake of August 17, 1999, were concentrated in a narrow band along the ground surface fault zone. Therefore, the primary reasons of the damage will be attributed to the near earthquake source effects, leaving aside the quality of buildings. However, the following examples will be out of above category. One example is the heavy damage of buildings in Avcilar, west of Istanbul, even relatively further (~150 km) from the source (e.g., Cranswick et al., 2000). In addition, the strong contrast of damage ratios between the strong motion observation site; Sakarya (SKR), and the downtown Adapazari, and wide variation of the damage ratios even in a relatively narrow area of Golcuk (the Architectural Institute of Japan Reconnaissance Team et al., 2000) are also similar issues. We have to remind poor construction of collapsed buildings, however, site effects on earthquake ground motion were plausibly significant on the damage in these areas.

A strong motion record is a key for understanding the damage and the earthquake source dynamics. The strong motion records from the Kocaeli earthquake were successfully recovered and quickly distributed through the Internet by the Earthquake Research Department, Directorate for Disaster Affairs of the Ministry of Public Works and Settlement (ERD) (1999), and Kandilli Observatory and Earthquake Research Institute (KOERI) (1999). The efforts were very valuable for scientists and engineers, as they could quickly understand the severity of ground motion during the earthquake. However, because of sparse network in Turkey (Celebi et al., 2000), no strong motion record was obtained at severely damaged areas, except Duzce (DZC). The surface geological and/or the geotechnical data near the strong motion observation sites and damaged areas are very limited, therefore, it is very hard to quantitatively interpret the variation of ground motion severity and its relation to earthquake damage.

It has been suggested that an S-wave velocity structure at a site is a most valuable data for understanding the site effects on ground motion. However, the methods for determining S-wave velocity structure for deep sedimentary basin are quite limited and any conventional geophysical exploration are hardly applicable to damaged areas just after a devastating earthquake. We, therefore, carried out array observations of microtremors aiming to determine the S-wave velocity structures beneath the strong motion observation sites and damaged areas. Additionally, we also conducted quite temporal array observations of aftershocks to understand the relative difference of site effects on strong motion or damage in and around Golcuk, near epicentral area, on September 1999, and at the Istanbul University in Avcilar, west of Istanbul.

## Array Observation of Microtremors

### Method

Pioneer works for determining velocity structure by using microtremors or microseisms were carried out by Aki (1957), Toksoz (1964), and Lacoss et al. (1969). The methods are provided for estimating velocity structures by using the phase velocity dispersion of surface waves included in microtremors. Asten and Henstridge (1984), Horike (1985), and Matsushima and Okada (1990) made efforts to increase the resolution of phase velocity determination by using array observation of microtremors, applying the frequency-wavenumber (f-k) analysis (Capon, 1969). Horike (1985) developed also an inversion method of obtained phase velocity of Rayleigh waves for determining S-wave velocity structure. Aki (1957) gave a theoretical basis of the spatial autocorrelation coefficient defined for microtremors data and developed a method to estimate phase velocity dispersion of surface waves contained in microtremors by using a specially designed circular array. Henstridge (1979) also introduced a licit expression of a relationship between the spatial autocorrelation coefficient and the phase velocity of fundamental-mode Rayleigh waves. The method has been extended to an exploration method by Okada et al. (1990),

Matsuoka et al. (1996), and Okada (1998), that is currently called SPAC method. The SPAC method has been employed throughout the present study. A flow of observation and analysis in the method is shown in Figure 1, and a principle of the method is given in Appendix.

We have carried out array microtremors measurements at the strong motion observation sites (ATS, CNA, YPT, SKR, and DZC) and damaged areas, such as Avcilar (ISU and AVC), Adapazari (ADC and ADU), Golcuk (GLF and GLH), and Degirmendere (DMD) at two different periods (September and December in 1999). Figure 2 shows the location map of the surveyed areas.

A circular array consisting of four (optionally seven) stations was used, which is a regular triangle-shape with a center, as shown in Figure 1. A size of an array was selected associated with the availability of space at a site. As shown in Table 1, plural arrays by changing sizes at different time were deployed, except SKR site, to cover wide wavelength or phase velocity change as a function of frequency. Generally speaking, measurements were restricted with narrow areas of observation rather than we expected, therefore, the resolution of determined phase velocities at low frequenc ies would be limited. We made measurements in daytime and an observation time duration of microtremors for one measurement was 30 minutes for small (L<100 m) arrays and 45 or 60 minutes for larger ones, respectively.

## Instruments

Five (optionally seven) sets of the portable seismographs (Kudo et al., 1998) were used for array microtremors measurements. The seismograph is originally developed for temporal observation of strong and weak earthquake motions. They are composed of a tri-axial accelerometer (Akashi Co. Ltd.) of highly damped (h~26) moving coil type (natural frequency of 3 Hz), signal conditioner (amplifier and filter), and a data logger (24 bits digitizer, 20 megabytes flash memory, and GPS time synchronization; Hakusan-Kogyo Co. Ltd.). A flat response (-3 dB) of ground acceleration is attained from 0.1 Hz to an aliasing frequency. The sensitivity of the sensor is 1 Volt/g and optionally 5 Volt/g; g denotes the gravity. Instruments were also used for aftershock observation without amplifying. The clipping level of sensor is 150 cm/sec; the maximum observable acceleration is 1 g at 1 Hz or 10 g at 10 Hz. The allowable input level of the data logger is selectable for 1 or 5 Volts. Total weight including an inner battery (2 kg) is 7 kg. The low-pass filter of cut-off frequencies at 2, 5, and 30 Hz is provided. We used the filter at cutoff frequency of 2 Hz for large arrays and 5 Hz for small ones in microtremors observation.

## Analysis and Results

We use only vertical motion of microtremors for aiming to extract Rayleigh waves. Figure 3 shows an example of the velocity time histories integrated from acceleration of microtremors that were simultaneously recorded at one place, their power spectra, and coherence. It is apparent that there is no use for instrumental correction in the higher frequency range than 0.1 Hz.

The integrated velocity computed from original acceleration was used in the following analysis. The SPAC coefficients at a frequency are calculated for each time blocks divided into every 81.92 seconds. The time block was chosen for over-rapping 21.92 seconds to the next block. Finally the SPAC coeffic ients were averaged. One example of the results for representative frequencies obtained at ATS is shown in Figure 4. The error bar in the figure shows the standard deviation of the SPAC coefficients obtained from 20 to 40 blocks. The quality of determined phase velocity is controlled by the degree of matching between the Bessel function and the observed SPAC coefficients against distances. The results are not so excellent, but satisfactory. Next, we will find a dispersion curve or S-wave velocity structure that fits to observed data by using the genetic algorithm (GA) (Yamanaka and Ishida, 1996). Circles as well as triangles in Figure 5 show the phase velocities determined by the SPAC method, while continuos lines show dispersion curves estimated by using the genetic algorithm with some

minor manual corrections. P-wave velocities are assumed corresponding to S-waves by using the empirical relation by Ludwig et al. (1970). Thus determined phase velocity dispersions at the sites and the estimated S-wave velocity (Vs) structures are shown in Figure 5 and Table 2. They are summarized as follows:

*West Istanbul*

ATS: Strong motion observation site run by the Kandilli Observatory and Earthquake Research Institute (KOERI). No significant damage was found in the building where strong motion instrument has been installed. S-wave velocities of surface layers increase from 200 m/sec to 1200 m/sec with depth (from surface down to 550 m). The high level and relatively long period accelerations from the mainshock can be attributed to those soft surface layers (Vs<400 m/sec).

ISU and AVC: These sites are close to the damaged area of Avcilar and their velocity structures are similar to that of ATS. Therefore, their ground motions during mainshock are supposed to be similar to that of ATS. This will be discussed later with the aftershock data.

CNA: Strong motion observation site run by KOERI. A thin (~15 m) low velocity (Vs~300 m/sec) layers exist near the surface, but high velocity (Vs>600 m/sec) layers are underlying at a shallow depth. The reason of high acceleration at CNA can be qualitatively interpreted by the existence of shallow thin surface layers of low S-wave velocity with high velocity contrast.

*Izmit Bay area*

YPT: Strong motion observation site run by KOERI. There was no distinctive damage in the buildings where the strong motion instrument has been installed. The S-wave velocity of surface layer is estimated to be 340 m/s and it increases with depth. The observed deepest layer having S-wave velocity of 950 m/sec is estimated at a depth of about 500 m.

GLF: The site is located in the eastern part of Golcuk where a big factory is under-construction. The area sank about two meters during or after the mainshock. The site has very thick (~80 m) sedimentary layers of which S-wave velocity of 150 and 260 m/sec. A rather high velocity (950 m/sec) layer is estimated at a depth of about 350 m.

DMD: The site is located near west of the Naval base and close to the west margin of the inland where surface fault was observed. Large number of medium-rise (higher than four stories) buildings were heavily damaged or collapsed near the site. Soft sediments (Vs<400 m/sec) are very thin compared with GLF and YPT.

GLH: The site is located on the hill of the south of damaged area in Golcuk. This area consisting of mostly low -rise buildings had slight damage. The S-wave velocities of layers to a depth of about 100 m are higher than the other sites near Golcuk.

*Adapazari City*

SKR: Strong motion observation site run by the Earthquake Research Department (ERD). The available area for array observation of microtremors was so narrow that one small array observation could be carried out. Dispersions of phase velocity were slight but the velocity itself was relatively high. The S-wave velocity of near surface is estimated to be approximately 1000 m/sec or higher.

ADC: The site is located on the heavily damaged area in Adapazari City, three kilometers northeast from SKR. A soft layer (Vs~230 m/sec) extends to a depth of about 40m. A thick (~100 m) and an intermediately hard layer (Vs~440 m/sec) underlie this soft layer.

ADU: The site is located on a few kilometers northeast from the heavily damaged area in downtown Adapazari City. The buildings at the surveyed area were mostly one or two stories and the damage was very light compared with downtown Adapazari. Very soft and thick layers with Vs of 170 and 330 m/sec cover the surface. It is not so definite, but total thickness of

sedimentary layers (Vs<1000 m/sec) is estimated to be 470 m.

The strong motion data from the mainshock cannot be directly used for interpretation of damage in the sedimentary basin extending in Adapazari City. This will be discussed later.

*Duzce*

DZC: Because there was no enough space to carry out the array observation of microtremors at the ERD strong motion site, we moved to one kilometer east from the site. Duzce suffered severe damage from the August earthquake as well as the November 12 earthquake (Mw7.2). The site is a sedimentary basin consists of thick and soft sediments at surface (Vs~260 m/sec) and intermediate depths (Vs~460-510 m/sec). We may also say that the ground motions during two large events were strongly affected by surface soils.

## Array Observation of Aftershocks in Golcuk

Quite temporal aftershock observations were carried out for understanding the site effects on ground motions in Golcuk City, where buildings were heavily damaged. The first array consists of three sites: on a hill in southeastern part of the city (GLS: no damage), near the Ataturk street of eastern Golcuk (GLA: heavy damage), and at lowland in Golcuk City (GLF: heavy damage). GLS is taken as hard soil or rock site and the others are sediment sites. The observation period was one night for north-south array and four days for the station YPT, where is a reference site. The second array observation was carried out at three stations (GLF, GLJ, and GLN) along the east-west direction near the coast of Golcuk. The intervals between stations in Golcuk were approximately 2 or 3 km. Table 3 shows the sites and observed events that were recovered at plural sites. The location map of stations is shown in Figure 6. The instruments are the same as those used for array observation of microtremors, but without an amplifier and filter.

An example of the observed record section is shown in Figure 7. The station GLF recorded most of the common events. Therefore, we used GLF as a reference; nevertheless the site effects at GLF are the largest among the observation sites. Spectral ratio method is our first approach. To apply the method, focal distance and radiation pattern corrections will be required. The source locations of the recorded events have not necessarily been determined. Therefore, we used S-P time for distance correction. A linear relation is obtained between focal distances computed using the source locations determined by KOERI (1999) and S-P times measured by our observation at GLS and GLF where the delays of arrival time due to sedimentary layers were corrected, as shown in Figure 8. To determine the focal distances at sediment sites, the arrival time was corrected by using the S-wave velocity structure determined by array observation of microtremors and the associated P-wave velocity (Vp) was assumed by the empirical Vp/Vs relation by Ludwig et al. (1970). Because structure models at GLJ, GLA, and GLS are not available, we assumed that the focal distance at GLJ was averaged using GLF and GLN, and the same ones of GLS were used for GLA. A radiation pattern effect is hardly removed, however, we assumed that the effect becomes small by vectorial summation of two horizontal components. Spectral ratios obtained through these observations are shown in Figure 9. Solid and gray lines show the average spectral ratios and the individuals, respectively (Figure 9a). If we take YPT as a reference site, the site responses in and around Golcuk are summarized as shown in Figure 9b. GLF and GLJ exhibit large responses relative to YPT at low frequency (0.5-0.6 Hz) and GLA shows very large site amplification at 1.5 and 4 Hz. On the other hand, site responses at GLN and GLS were smaller than YPT below 3.5Hz. A large response of GLS at high frequency would be caused by shallow surface soil. It is not easy to interpret the relation between site amplification and damage ratio. However, based on the detailed inventory survey of buildings in Golcuk and Degirmendere by Architectural Institute of Japan Reconnaissance Team et al. (2000),

the high collapse ratios of medium-rise buildings near GLF and GLJ correlate with the aftershock and microtremors data.

## Estimation of Ground Motion at Avcilar

One of the significant questions about the present earthquake is why severe damage of buildings in Avcilar, west of Istanbul occurred (Cranswick et al., 2000). One of the possible reasons will be fragility of buildings; however, is that an only reason? The strong ground motion during the mainshock at ATS, near Avcilar, showed large amplification compared with other sites in west of Istanbul, e.g. CNA. Their velocity seismograms and acceleration spectra are compared in Figure 10 and we can identify the large difference between them, nevertheless the epicentral distances are almost the same.

We have temporally installed a portable accelerograph without amplifier on a basement of building in the campus of Istanbul University (ISU). The building was moderately damaged during the mainshock. The ground motions from the Marmara Sea earthquake of October 20 (M=4.4, 40.76N, 28.94E, Depth=9.6 km determined by KOERI) were recorded at this site as well as at both CNA and ATS. The acceleration time histories are shown in Figure 11. Figure 12(a) shows the Fourier spectral amplitudes at CNA and ATS during the mainshock on August 17, 1999 along with those at CNA, ATS, and ISU during the event (M 4.4) on October 20, 1999. Figure 12(b) shows the spectral ratios of CNA to ATS for the mainshock and those of CNA and ISU to ATS for the event on October 20, 1999. These figures show that the spectral ratios (CNA/ATS) have no significant difference between the strong motion from the mainshock and the weak motion from the M4.4 event; this implies that the effects of distance, azimuth, and non-linearity of soils are small or negligible at CNA and ATS. Figures 10 and 12(b) indicate that ATS is amplified by a factor of 5-10 compared with CNA at lower frequency than 4 Hz, on the other hand, the relation becomes reverse in the high frequency range. Gray lines in Figure 12(b) indicate that the ground motions at ISU and ATS are comparable. Cranswick et al. (2000) has suggested a large amplification of ground motion in the longer period than 4 sec in Avcilar, however, they obtained similar result with us in shorter periods than 1 sec.

We estimated strong ground motion during the mainshock in damaged area using underground structures determined by array observations of microtremors and earthquake motion observed near the damaged areas. First, we estimated the incident wave at ATS by deconvolving the responses of the surface layers from the record of the M4.4 event based on 1D S-wave propagation theory by using the velocity structure model estimated by microtremors (see Table 2 or Fig. 5). Next, the estimated input motion is convolved with the velocity structure model at ISU, assuming the common input motion at the layer of S-wave velocity of 1230 m/sec. Thus obtained synthetic transverse motion is compared with the observation as shown in Figure 13. Later arrivals are not well simulated, but major early S-wave arrivals are satisfactory. The S-wave velocity models with assuming constant Q are shown in Table 4. As we could not find any significant effects of non-linearity at ATS during mainshock (Fig. 12), a similar approach for the mainshock will be permitted. The estimated transverse motions during the mainshock at ISU and AVC are compared with that of ATS in Figure 14. The ground acceleration at AVC is lowest among them; however, the differences are not so significant.

## Estimation of Ground Motion in the Adapazari Basin

The strong ground motion at downtown Adapazari is also a matter of our concern, because no strong motion record was obtained in the fast-growing urban/industrial area of the Adapazari

basin where buildings were severely damaged (Celebi et al., 2000). Principally, a similar approach to the case of Avcilar may not be suitable for estimating ground motion at Adapazari area, because it plausibly includes near source and non-linear effects of soft soil during strong shaking. First, we estimated ground motions during the mainshock at ADC and ADU where S-wave velocity structure models have been estimated (Fig. 5 and Table 4) similar to the case of Avcilar. That is, the EW component of the ground motion at SKR deconvolved by the response of the surface layer is used for an input motion at ADC and ADU and the synthetic motions at ADC and ADU are estimated by convolving the sedimentary layers determined by microtremors. The velocity models and Q factors used in the computation are shown in Table 4. Figure 15 shows the synthetic ground accelerations and velocities at ADC and ADU, assuming 1D propagation of S-wave without any corrections of distance and non-linearity. The synthetic motions will only be valuable as an upper band of estimation at the sites. The distances at SKR, ADC, and ADU from the nearest surface fault line were 3.4, 6.4, and 9.6 km, respectively. The peak acceleration (582 cm/sec$^2$) and velocity (108 cm/sec) at ADC will be reduced to 488 cm/sec$^2$ and 74 cm/sec, respectively, using the relative distance relation with the help of the empirical formula (Joyner and Boore, 1982). In case of ADU, those will become to 368 cm/sec$^2$ and 61 cm/sec, respectively.

Our next concern is non-linear effects on strong ground motion. Liquefaction was observed in downtown Adapazari; however, it was not evident at ADC and ADU. During the 1995 Hyogo-ken Nambu earthquake, nonlinear effects on ground motion were not so significant at least several seconds after S-wave arrival or before the occurrence of liquefaction (Aguirre and Irikura, 1997). In addition, the non-linearity of ground was not an essential effect for the long period ground motions recorded at Niigata City where liquefaction was observed during the 1964 Niigata earthquake (Kudo et al, 2000). The estimated ground motions at ADC and ADU dominate in longer period than 1 second; therefore, we are not necessary to make drastic corrections, at least for long period motions in ADC and ADU. Our discussion is restricted in qualitative due to non-availability of soil dynamic and other necessary data; therefore, we have to despair of further corrections especially for short period motion.

Although the effects of 2D or 3D effects are not taken into account, because of too sparse of geotechnical data in the Adapazari basin, the estimation of ground motions as an upper band will possibly be corrected.


**Discussion**


It is a matter of our concern to understand the severity of the estimated ground motions at Avcilar (AVC and ISU) and in Adapazari basin (ADC and ADU) relative to the strong motions that have ever been recorded. Figure 16 compares the pseudo velocity response spectra (h=5%) of simulated motions with those of some records that have been used in earthquake engineering.

The left of Figure 16 shows the response spectra calculated from the simulated motions at ISU and AVC and those obtained from the recorded motions at ATS. They are compared with those of El Centro from the 1940 Imperial Valley earthquake (Ms 7.1) and Hachinohe from the 1968 Tokachi-Oki earthquake (M 7.8). The response spectra of ISU, AVC, and ATS are comparable in amplitude with those of El Centro and Hachinohe at periods shorter than 2 sec. The amplitudes of the response spectra in the period range are most significant for low- and medium- rise buildings. In fact many reinforced concrete buildings near the strong notion site were severely damaged during the Tokachi-oki earthquake. As a result, this earthquake became trigger for the revision of the building code in Japan. The buildings with similar quality are still used in Japan as well as everywhere in the world.

The right of Figure 16 shows the response spectra calculated from the simulated motions at

ADC as well as ADU and the recorded motions at SKR together with those of Kobe (JMA) from the 1995 Hyogo-ken Nambu earthquake. The thick broken and solid lines indicate the response spectra at ADC with and without distance correction, respectively. In the distance correction, the empirical relationship by Joyner and Boore (1982) was referred to. Similarly, the gray broken and solid lines also indicate those at ADU with and without distance correction. The simulated velocity responses of ADC after a distance correction are comparable to those of Kobe at a period around 2 sec. Those in the period range from 1 to 1.5 sec. are almost 50 % of Kobe but exceeding 100 cm/sec. Roughly saying, the velocity responses of ADC are two times larger than those of SKR in the frequency range from 0.5 to 3 sec. Such ground motions at ADC would be very serious for medium- and high-rise buildings. A very high contrast of building damage between SKR and ADC or downtown Adapazari could probably be attributed to the difference of the site response.

## Conclusion

We conclude that the array observation of microtremors is very promising method for determining S-wave velocity structures from shallow to intermediate depths, especially at damaged areas in sediment sites, while the array observation of aftershocks allow us to directly compare site responses. A linkage of S-wave velocity structure and aftershock data provides for quantitative evaluation of site responses. A large and long duration of strong motion records at ATS are closely related to the low velocity (Vs=200 m/sec) of soft surface layers. The sedimentary layers in Avcilar (ISU and AVC) are similar to those of ATS, so that the ground motion at Avcilar during the mainshock may be similar to that of ATS. Aftershock data prove actually this estimation. The ground motion at a period around 1 sec (response of 60-80 cm/sec) is comparable to those of El Centro (1940) and Hachinohe (1968) that have been used for building design in Japan. At Hachinohe, the damage of RC-building was especially severe during the 1968 Tokachi-oki earthquake.

Through the array observations of microtremors, it becomes evident that SKR is located on very hard soil (Vs >1000 m/sec), while thick soft sediments cover the downtown and its extent (ADC and ADU). The ground motion at ADC in downtown Adapazari during the mainshock is estimated to be two or three times larger than that of SKR. Especially large amplifications in the period range from 1 to 2 sec were very severe to medium-rise buildings near ADC.

A large difference of strong motions between a hillside and Izmit Bay area in and around Golcuk is also indicated by the comparison of aftershock records. However, it is still necessary to investigate more detailed underground structures for understanding the difference of damage ratios in the downtown of Golcuk.

## Acknowledgements

# REFERENCES

Aguirre, J. and K. Irikura (1997). Nonlinearity, liquefaction, and velocity variation of soft soil layers in Port Island, Kobe, during the Hyogo-ken Nanbu earthquake, *Bull. Seism, Soc. Am.* **87**, 1244-1258.

Aki, K. (1957). Space and time spectra of stationary stochastic waves, with special reference to microtremors, *Bull. Earthq. Res. Inst.* **35**, 415-456.

Architectural Institute of Japan Reconnaissance Team with Bogazici University, Istanbul Technical University, and Middle East Technical University (2000). Progress report on damage investigation after Kocaeli earthquake by Architectural Institute of Japan, *International Journal for Housing Science and Its Applications* **24**, 97-126.

Asten, M. and J. D. Henstridge (1984). Array estimators and the use of microseisms for reconnaissance of sedimentary basins, *Geophysics* **49**, 1828-1837.

Capon, J. (1969). High-resolution frequency-wavenumber spectrum analysis, *Proc. IEEE* **57**, 1408-1418.

Celebi, M., S. Toprak, and T. Holzer (2000). Strong-motion, site-effects and Hazard Issues in rebuilding Turkey: in light of the 17 August, 1999 earthquake and its aftershocks, *International Journal for Housing Science and Its Applications*, **24**, 21-38.

Cranswick, E., O. Ozel, M. Meremonte, M. Erdik, E. Safak, C. Mueller, D. Overturf, and A. Frankel (2000). Earthquake damage, site response, and building response in Avcilar, west of Istanbul, Turkey, *International Journal for Housing Science and Its Applications* **24**, 85-96.

Earthquake Research Department, Directorate for Disaster Affairs of the Ministry of Public Works and Settlement (ERD) (1999). *http://www.deprem.gov.tr/main_e.htm*.

Henstridge, J. D. (1979). A signal processing method for circular array, *Geophysics* **44**, 179-184.

Horike, M. (1985). Inversion of phase velocity of long-period microtremors to S-wave-velocity structure down to the basement in urbanized areas, *J. Phys. Earth.* **33**, 59-96.

Joyner, W. B. and D. M. Boore (1982). Prediction of earthquake response spectra, *USGS Open-file rep.*, **82-977**, 1-16.

Kandilli Observatory and Earthquake Research Institute (KOERI) (1999). *http://kandilli.koc.net/earthquake.htm*.

Kudo, K., M. Takahashi, M., Sakaue, T., Kanno, H. Kakuma, and D. Tsuboi (1998). A highly over-damped moving coil type accelerometer for mobile strong motion observation and its performance tests, *Report of Grant-in-Aid for Scientific Research-07558056*, *in Japanese with English abstract*.

Kudo, K., T. Uetake, and T. Kanno (2000). Re-evaluation nonlinear site response during the Niigata earthquake using the strong motion records at Kawagishi-cho, Niigata city, *Proc. The Twelfth World Conf. Earthq. Eng.*, **CD-ROM**, Paper No. 969/4/ A

Lacoss, R. T., E. J. Kelly, and M. N. Toksoz (1969). Estimation of seismic noise structure using arrays, *Geophysics* **34**, 21-38.

Ludwig, W. J., J. E. Nafe, and Drake (1970). Seismic refraction, *The Sea* **4-1**, 53-84.

Matsuoka, T., N. Umezawa, and H. Makishima (1996). Experimental studies on the applicability of the spatial autocorrelation method for estimation of geological structures using microtremors, *BUTSURI-TANSA* **49**, 26-41, *in Japanese with English abstract*.

Mtsushima, T. and H. Okada (1990). Determination of deep geological structures under urban areas, *BUTSURI-TANSA* **43**, 21-33.

Okada, H., T. Matsushima, T. Moriya, and T. Sasatani (1990). An exploration technique using long-period microtremors for determination of deep geological structures under urbanized areas, *BTSURI-TANSA* **43**, 402-417, *in Japanese with English abstract*.

Okada, H. (1998). Microtremors as an exploration method, Geo-exploration handbook, *Soc. Exploration Geophysicists of Japan* **2**, 203-211, *in Japanese*.

Priestley, M. B. (1981). Spectral Analysis and Time Series, *Academic Press* **vol. 2**, 718-720.

Toksoz, M. N. (1964). Microseisms and an attempted to exploration, *Geophysics* **29**, 154-177.

Yamanaka, H. and H. Ishida (1996). Application of genetic algorithms to an inversion of surface-wave dispersion data, *Bull. Seism. Soc. Am.* **86**, 436-444.

**Appendix**

Array observation of microtremors is potentially a method of gaining information on underground structures beneath a site where a seismometer array is deployed The method is basically to extract surface waves from microtremors in a form of dispersion, and then to invert the dispersion to an underground structure. Practically, the vertical component of fundamental-mode Rayleigh waves is a direct object of extraction.

To extract surface waves from microtremors, two methods are available ; they are the frequency (f)-wavenumber (k) power spectral density method (f-k method) (e.g. Asten and Henstridge, 1984; Capon, 1969; Lacoss et al., 1969) and the spatial autocorrelation coefficient method (SPAC method) (Aki, 1957; Okada, 1998). Both f-k and SPAC methods are based on the assumptions that microtremors are spatio-temporally stationary stochastic process. SPAC method, furthermore, needs such an assumption that microtremors are predominated by a single mode of surface waves.

We employed the SPAC method, because it has such an advantage over the f-k method; the SPAC method only requires fewer stations and smaller array than the f-k method to arrive at the similar result. The method employs a special seismic array that consists of vertical component seismometers placed on a circle with a seismometer placed at the center. Practically, 3 seismometers at least should be equally spaced on a circle so that these form an equilateral triangle array.

The microtremors as a stationary stochastic process are mathematically expressed in the polar coordinate system. Here we define the spatial autocorrelation function $S(r,\theta)$ between microtremors $X(t,0,0)$ at the center $(0,0)$ of a circular array with a radius $r$ and $X(t,r,\theta)$ at an observation station $(r,\theta)$ on the circumference of the circular array.

$$S(r,\theta) \;?\; E[X^*(t,0,0)X(t,r,0)]$$

$$?\; \lim_{T\to\infty}\frac{1}{2T}\int_{-T}^{T} X^*(t,0,0)X(t,r,\theta)dt \qquad\qquad \text{A1}$$

where $^*$ designates complex conjugate. Microtremors $X(t,r,\theta)$ as a stationary stochastic process are expressed as (Priestly [1981]);

$$X(t,r,\theta)\;?\;\int_{-\infty}^{\infty}\int_{0}^{\infty}\int_{0}^{2\pi}\exp\{i\omega t ? irk(\omega)\cos(\phi ? \theta)\}d?(\omega,k,\phi) \qquad\qquad \text{A2}$$

where $\phi$ is the direction from which the waves concerned arrive in array. The stochastic process $?$ satisfies the following orthogonal properties:

i)  $E[d?(\omega,k,\phi)]\;?\;0$, for all $\omega,k,\phi$ \qquad\qquad A3

ii)  $E[|\,d?(\omega,k,\phi)\,|^2]\;?\;dH(\omega,k,\phi)$, for all $\omega,k,\phi$ \qquad\qquad A4

iii)  for two different values of $\omega$ and $\omega'(\omega ? \omega')$ and two different values of $(k,\phi)$ and $(k',\phi')(k ? k',\phi ? \phi')$,

$$E[d?^*(\omega,k,\phi)d?(\omega',k',\phi')]\;?\;0 \qquad\qquad \text{A5}$$

where $H$ is the integrated spectra of microtremors. As the spectra of microtremors are generally continuous and able to differentiate, the stochastic process $?(\omega,\phi)$ in equation A4 satisfy the following property:

$$E[|\,d?(\omega,\phi)\,|^2]\;?\;dH(\omega,\phi)\;?\;h(\omega,\phi)d\omega\,d\phi \qquad\qquad \text{A6}$$

where $h(\omega,\phi)$ may be called "frequency-direction spectrum density function". When the average of the total power is integrated with respect to all the directions, the power spectral density function (or power spectrum) of microtremors at one station $h_0(\omega)$ is obtained as:

$$h_0(\omega)\;?\;\int_{0}^{2\pi} h(\omega,\phi)d\phi \qquad\qquad \text{A7}$$

Substituting equation A2 for equation A1 and using equations A3~A6, the spatial autocorrelation

function is rewritten as;

$$S(r,\phi) = \int_{-\pi}^{\pi} \int_0^{2\pi} \exp\{irk\cos(\theta-\phi)\}h(\omega,\theta)d\theta\, d\phi \qquad \text{A8}$$

Next, we define the "spatial autocorrelation coefficient at the angular frequency $\omega$" $\rho(\omega,r)$, as the averaged spatial covariance function normalized with the power spectrum of microtremors at one station within the array space (for instance, the center of the circular array), $h_0(\omega)$;

$$\rho(\omega,r) = \frac{1}{2\pi}\int_0^{2\pi} S(\omega:r,\phi)d\phi \Big/ h_0(\omega)$$

$$\qquad \text{A9}$$

$$= \frac{1}{2\pi}\int_0^{2\pi} \exp\{irk\cos(\theta-\phi)\}d\phi$$

Finally, we obtain;

$$\rho(\omega,r) = J_0(rk) = J_0(2\pi f r/c(f)) \qquad \text{A10}$$

since, $J_0$ is the Bessel function of the first kind of zero order and $k=\omega/c(\omega)$ where $c(\omega)$ is the phase velocity. Therefore, the spatial autocorrelation coefficient at the frequency $f$ is related to the phase velocity $c(f)$ via the Bessel function of the first kind of zero order.

As it is clear from the above theoretical consideration, the phase velocity at a certain frequency can be calculated by the spatial autocorrelation coefficient of the component wave of $\omega$, from the record of microtremors by a circular array with a radius $r$, by fitting the Bessel function using least square method.

Table 1.　Sites where the array observations of microtremors were carried out and the array sizes (L: length of one side of a triangle).

| Site Name | Code | Latitude | Longitude | Array Size L (m) Sept., 1999 | Array Size L (m) Dec., 1999 |
|---|---|---|---|---|---|
| Ambarli | ATS | 40.976 | 28.687 | 25, 100, 200 | |
| Avcilar (Istanbul Univ.) | ISU | 40.991 | 28.723 | 100, 200 | 25, 50 |
| Avcilar | AVC | 40.981 | 28.736 | | 25, 100 |
| Cekmece | CNA | 41.017 | 28.759 | 25, 100, 200 | |
| Table 1.  Yarmca | YPT | 40.764 | 29.762 | 25, 200, 500 | |
| Degirmendere | DMD | 40.726 | 29.798 | | 25, 100, 200, 346 |
| Glocuk | GLH | 40.708 | 29.834 | | 29, 100, 200 |
| Glocuk (Ford-Otosan) | GLF | 40.721 | 29.849 | 25, 100, 200 | |
| Adapazari | SKR | 40.737 | 30.381 | 50 | |
| Adapazari | ADC | 40.787 | 30.419 | | 25, 100, 200 |
| Adapazari | ADU | 40.753 | 30.411 | 100, 200 | 25, 400 |
| Duzce | DZC | 40.825 | 31.192 | | 50, 200, 400 |

Table 2.　Estimated S-wave velocity structures by array observations of microtremors.

| ATS Vs (m/s) | Thickness (m) | ISU Vs (m/s) | Thickness (m) | AVC Vs (m/s) | Thickness (m) | CNA Vs (m/s) | Thickness (m) |
|---|---|---|---|---|---|---|---|
| 204 | 32 | 225 | 18 | 291 | 46 | 311 | 15 |
| 364 | 57 | 370 | 75 | 434 | 91 | 613 | 32 |
| 608 | 164 | 584 | 197 | 584 | 267 | 778 | 42 |
| 919 | 295 | 919 | 188 | 919 | inf. | 1018 | 66 |
| 1018 | 100 | 1018 | 164 | | | 1230 | 141 |
| 1230 | inf. | 1230 | inf. | | | 1500 | inf. |

| YPT Vs (m/s) | Thickness (m) | DMD Vs (m/s) | Thickness (m) | GLH Vs (m/s) | Thickness (m) | GLF Vs (m/s) | Thickness (m) |
|---|---|---|---|---|---|---|---|
| 344 | 42 | 283 | 19 | 303 | 22 | 150 | 14 |
| 445 | 94 | 512 | 52 | 455 | 60 | 259 | 70 |
| 591 | 90 | 694 | 97 | 594 | 295 | 531 | 270 |
| 727 | 290 | 752 | 61 | 950 | inf. | 950 | 300 |
| 950 | 200 | 950 | 203 | | | 1120 | inf. |
| 1120 | inf. | 1120 | inf. | | | | |

| SKR Vs (m/s) | Thickness (m) | ADC Vs (m/s) | Thickness (m) | ADU Vs (m/s) | Thickness (m) | DZC Vs (m/s) | Thickness (m) |
|---|---|---|---|---|---|---|---|
| 1050 | 72 | 234 | 38 | 166 | 44 | 257 | 36 |
| 1500 | 56 | 441 | 97 | 331 | 88 | 459 | 44 |
| 2000 | inf. | 728 | 242 | 500 | 281 | 514 | 48 |
| | | 1500 | 70 | 878 | 63 | 769 | 236 |
| | | 2000 | inf. | 1050 | 100 | 1020 | 273 |
| | | | | 1500 | inf. | 1268 | 309 |
| | | | | | | 1500 | inf. |

Table 3.          Temporal aftershock observation sites and the observed aftershocks.

| EQ. No. | | | | 13 | 17 | 19 | 20 | 22 | 23 | 24 | 25 | 31 | 21 |
|---|---|---|---|---|---|---|---|---|---|---|---|---|---|
| Date (Local Time) | | | | 9/12 | 9/13 | 9/13 | 9/13 | 9/15 | 9/15 | 9/15 | 9/15 | 9/16 | 9/13 |
| Time (Local Time) | | | | 19:20:22 | 00:37:37 | 06:11:46 | 06:15:33 | 00:31:32 | 04:00:26 | 05:46:57 | 06:01:26 | 04:26:42 | 14:55:25 |
| Site Name | Code | Lat. | Long. | | | | | | | | | | |
| GLK-HILL | GLS | 40.694 | 29.873 | • › | • › | • › | • › | × | × | × | × | × | × |
| GLK-ARMY | GLA | 40.706 | 29.869 | × | • › | • › | • › | × | × | × | × | × | × |
| GLK-FORD | GLF | 40.721 | 29.849 | • › | • › | • › | • › | • › | • › | • › | • › | • › | × |
| YPT-TEMP | YPT | 40.764 | 29.762 | • › | • › | • › | • › | × | • › | × | × | × | • › |
| GLK-JDM | GLJ | 40.723 | 29.822 | × | × | × | × | × | • › | • › | • › | • › | × |
| GLK-NVM | GLN | 40.725 | 29.804 | × | × | × | × | • › | • › | • › | • › | • › | × |

Table 4.    S-wave velocity structure model used for synthetic ground motion.

| ATS | | | ISU | | | AVC | | |
|---|---|---|---|---|---|---|---|---|
| Vs (m/s) | Thickness (m) | Q | Vs (m/s) | Thickness (m) | Q | Vs (m/s) | Thickness (m) | Q |
| 204 | 32 | 15 | 225 | 18 | 20 | 291 | 46 | 25 |
| 364 | 57 | 30 | 370 | 75 | 30 | 434 | 91 | 40 |
| 608 | 164 | 60 | 584 | 197 | 50 | 584 | 267 | 50 |
| 919 | 295 | 200 | 919 | 188 | 200 | 919 | 188 | 200 |
| 1018 | 100 | 200 | 1018 | 164 | 200 | 1018 | 164 | 200 |
| 1230 | inf. | 200 | 1230 | inf. | 200 | 1230 | inf. | 200 |

| SKR | | | ADC | | | ADU | | |
|---|---|---|---|---|---|---|---|---|
| Vs (m/s) | Thickness (m) | Q | Vs (m/s) | Thickness (m) | Q | Vs (m/s) | Thickness (m) | Q |
| 1050 | 72 | 200 | 234 | 38 | 20 | 166 | 44 | 15 |
| 1500 | inf. | 200 | 441 | 97 | 40 | 331 | 88 | 30 |
| | | | 728 | 242 | 70 | 500 | 281 | 50 |
| | | | 1500 | inf. | 200 | 878 | 63 | 80 |
| | | | | | | 1050 | 100 | 200 |
| | | | | | | 1500 | inf. | 200 |
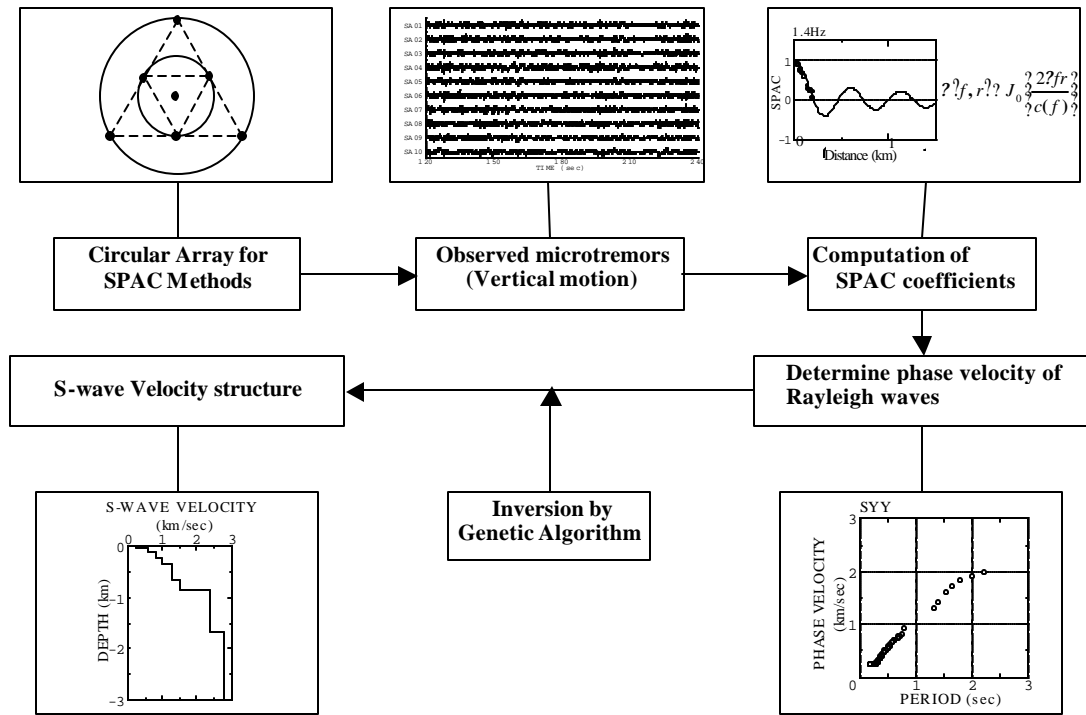
Figure 1.     A flow of observation and analysis in the SPAC method for estimating S-wave velocity structures using array observations of microtremors.
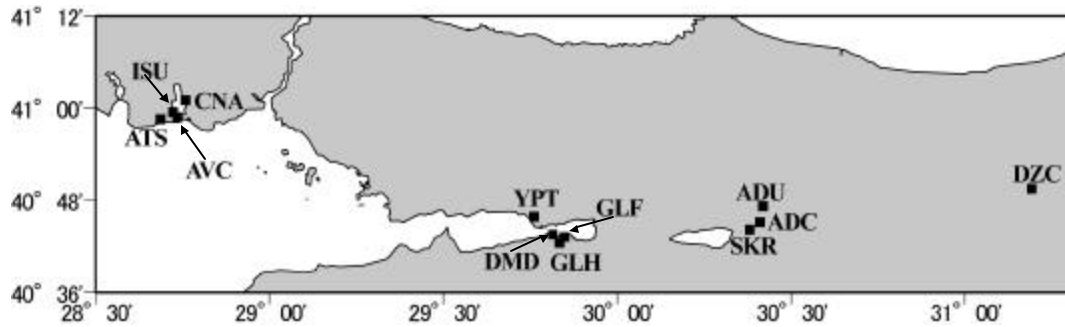


Figure 2.     A location map of the sites where array observations of microtremors were carried out
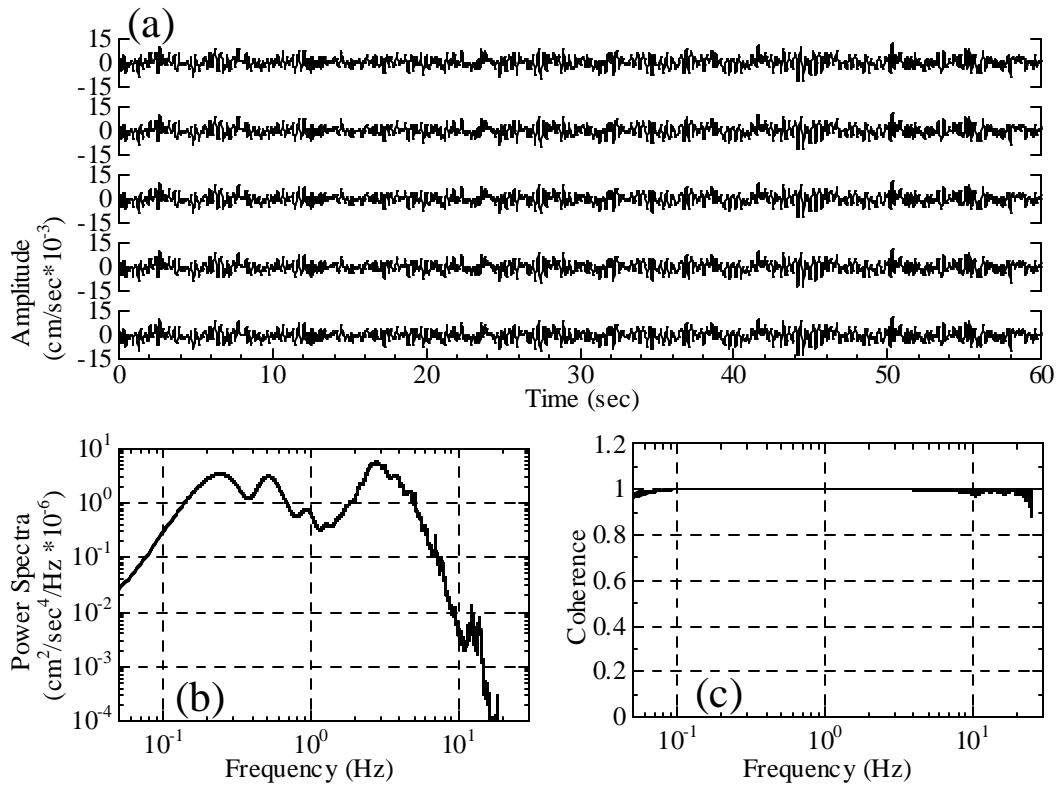
Figure 3.    Velocity waveforms of microtremors integrated from simultaneously recorded accelerations at one place (a), power spectra of observed accelerations (b), and the coherence (c).
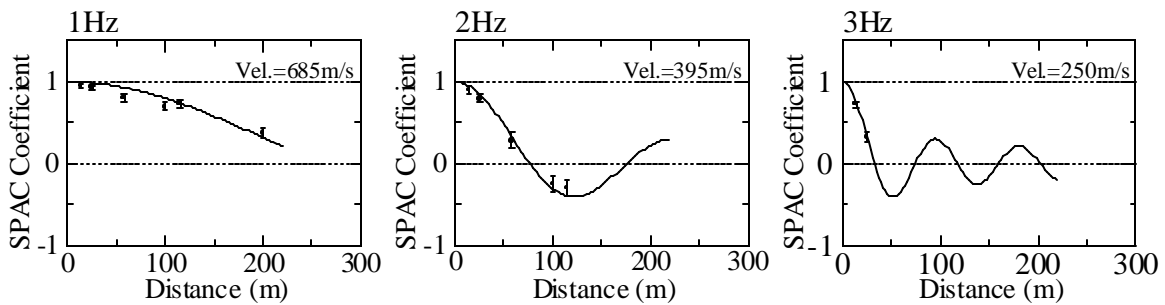


Figure 4.    Examples of the Bessel function fitted to the SPAC coefficients at ATS for some representative frequencies. The solid lines show fitted Bessel function and circles and the error bars indicate the SPAC coefficients and their standard deviations, respectively.
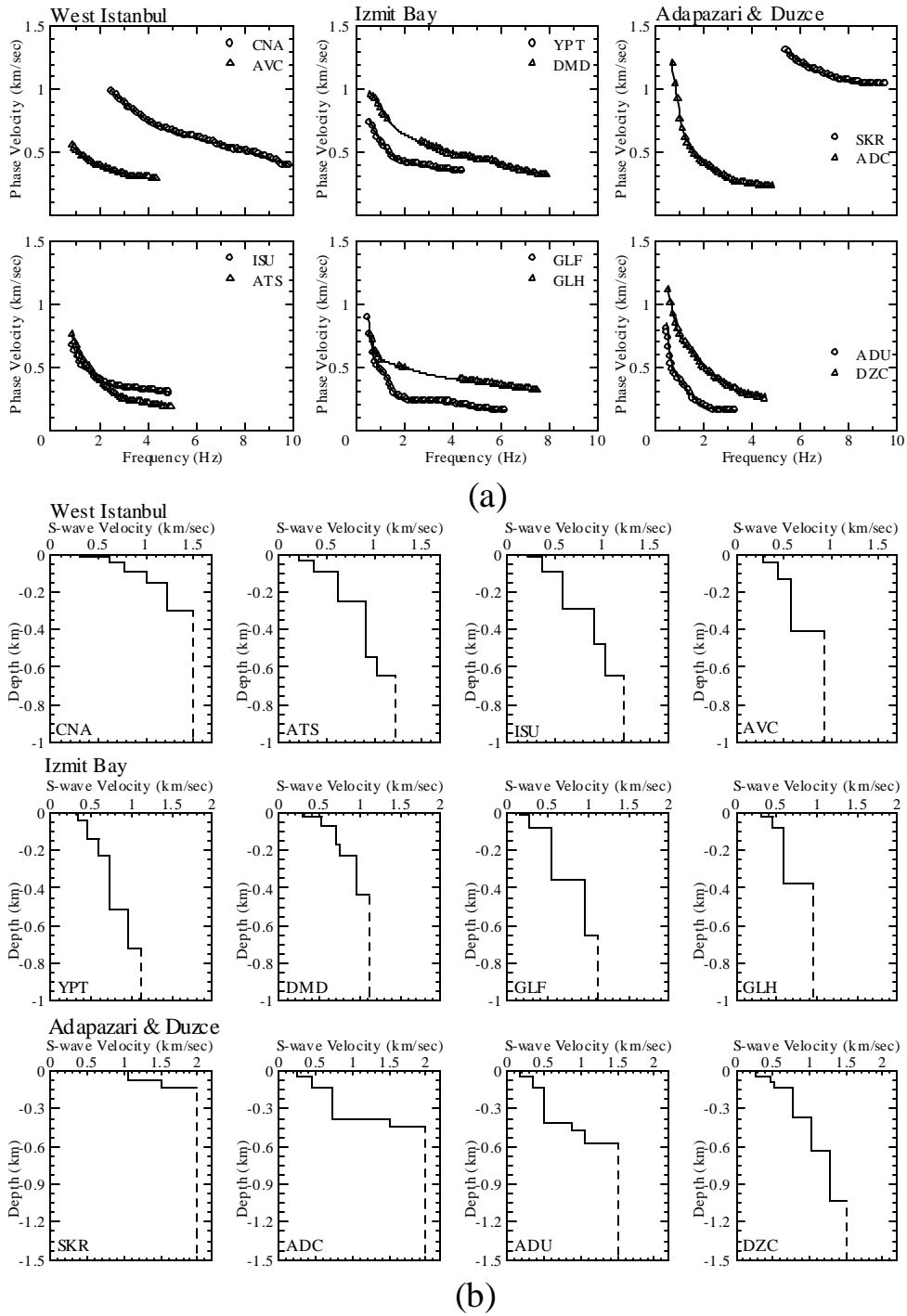
Figure 5.      Phase velocity dispersions of Rayleigh waves determined by array observations of microtremors at the surveyed area (a) and the corresponding estimated S-wave velocity structures (b). Circles as well as triangles and continuous lines in (a) show the observations and the computed dispersions obtained by using the genetic algorithm with minor manual modifications.
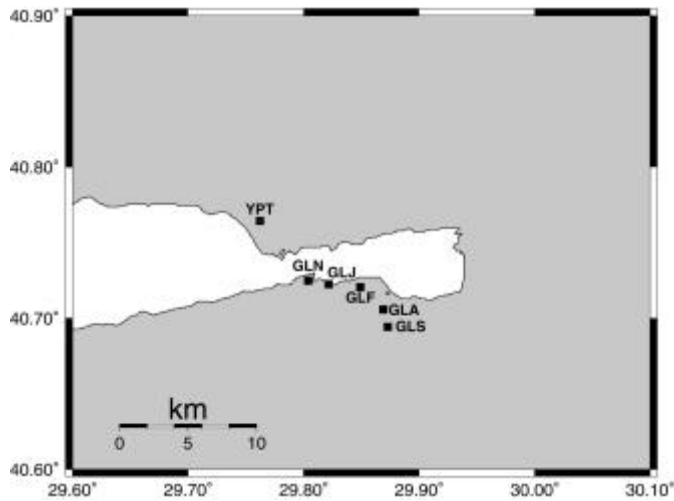
Figure 6.        A location map of aftershock observation sites in the Izmit bay area. GLS is located on a hill that is geologically old formation (MTA, Geology map) and the others are flat area of young sediments.
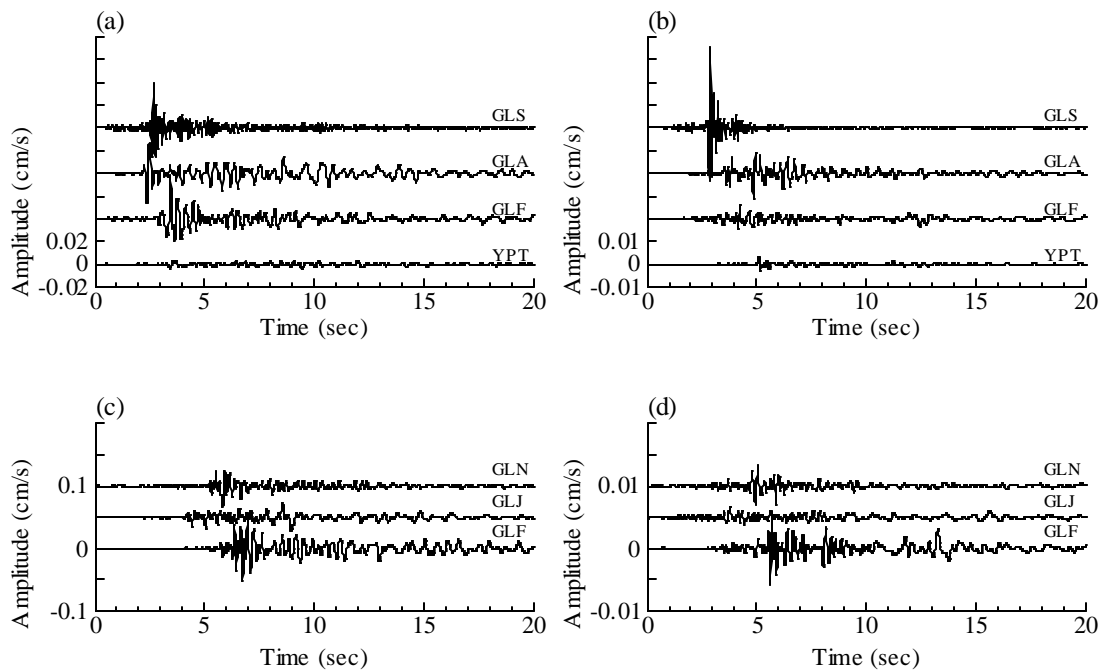


Figure 7.        Examples of waveforms from aftershocks. Record sections of integrated velocity of NS components by filtering with pass-band between 1-10Hz from the events 13 (a), 20 (b), 31 (c), and 25 (d) in Table 3. GLS predominate high frequency motion, while GLF is characterized by low frequency and long duration.
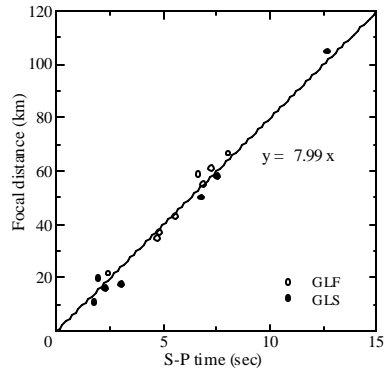
Figure 8.        Relations between S-P time and focal distance using the aftershock data at
GLS and GLF. At GLF, S-P times were corrected for the time delays due to the sedimentary layers.
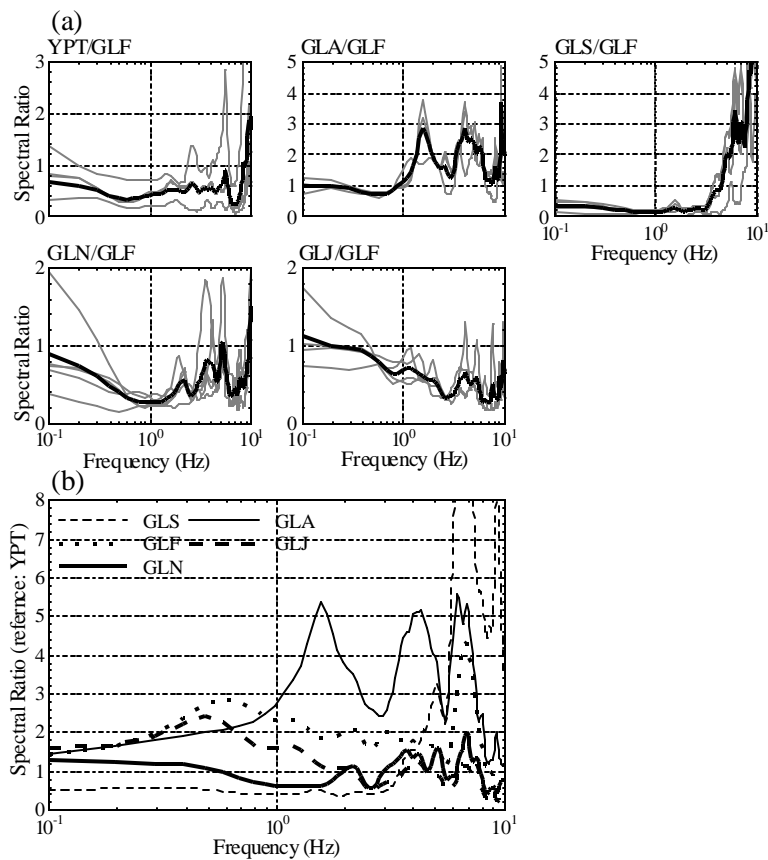


Figure 9. (a):        Spectral ratios of YPT, GLA, GLS, GLN, and GLJ to GLF obtained by aftershock data.
The spectra were obtained by vectorial summation of two horizontal components Solid and thin gray lines
show the average and the individual ratio, respectively. (b): Recalculated spectral ratios referring to YPT.
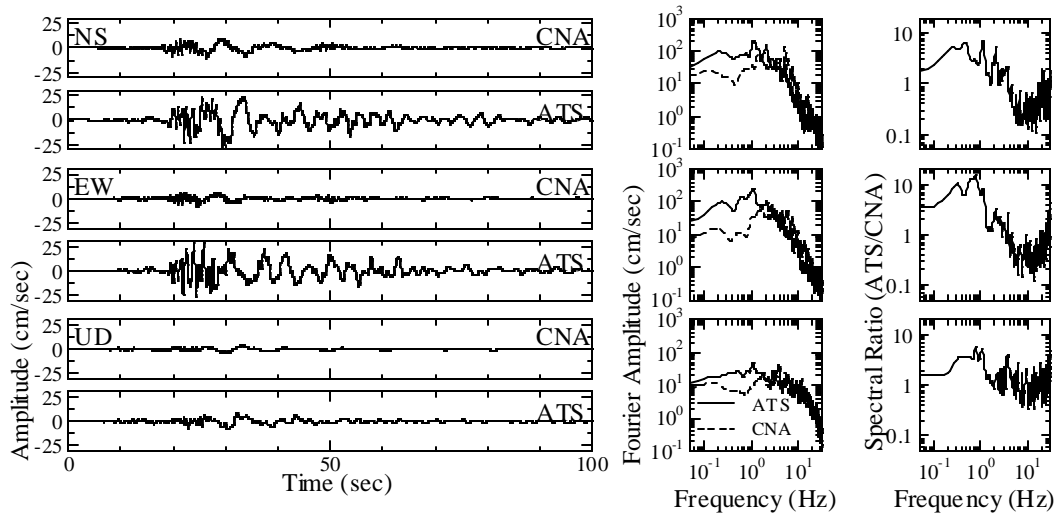
Figure 10. Comparisons of velocity seismograms and spectra at ATS and CNA, west of Istanbul.
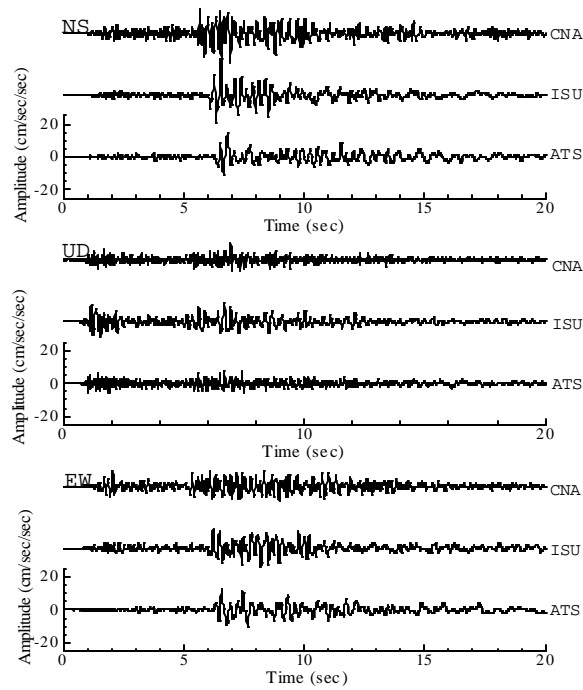


Figure 11. Acceleration time histories from the Marmara Sea earthquake of October 20 (M4.4) observed at CNA, ATS, and ISU
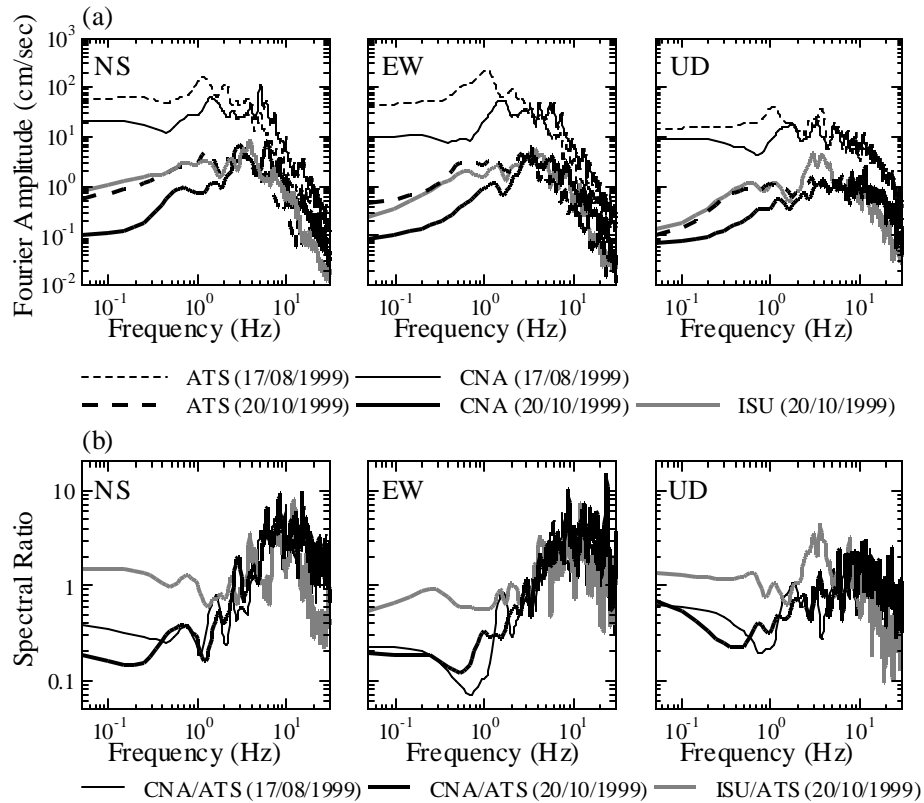
Figure 12. (a): Spectral amplitudes of CNA and ATS during the mainshock of August 17 are shown by thin broken and solid lines, respectively. Thick solid, broken, and gray lines show those of CNA, ATS and ISU from the October 20 event (M4.4), respectively. (b): spectral ratios of CAN and ISU to ATS showing both for the mainshock and the M4.4 earthquake.
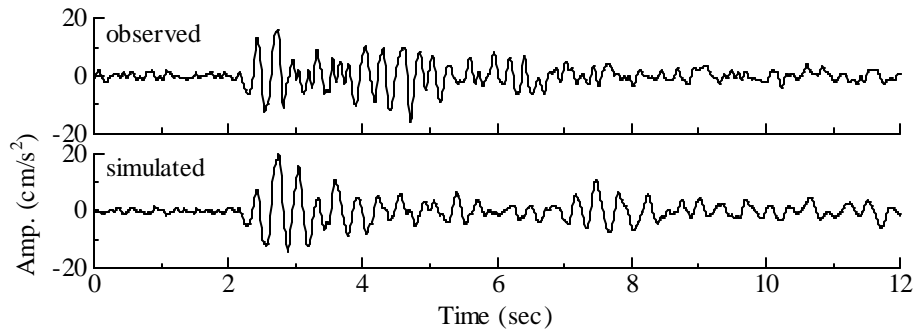


Figure 13.    Synthetic transverse ground acceleration at ISU for the Marmara Sea earthquake of October 20 (M4.4) is compared with the observed ones. A good match was obtained at least initial part of S-wave arrival.
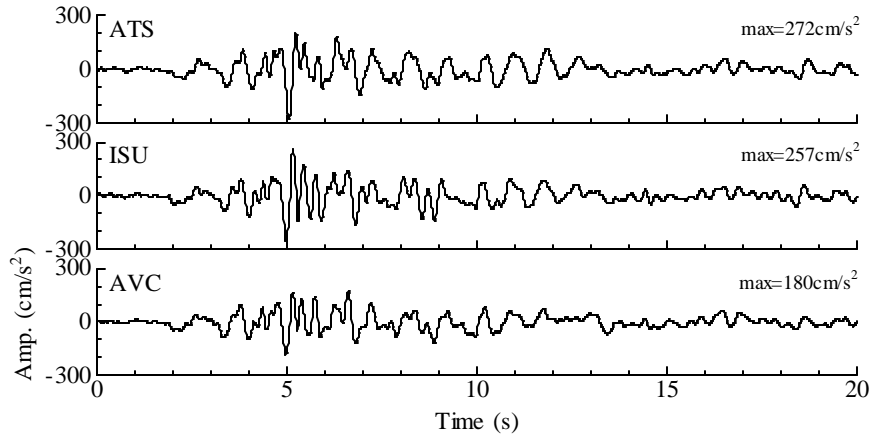
Figure 14.　　　　Synthetic transverse accelerations at ISU and AVC are compared with the observed acceleration at ATS
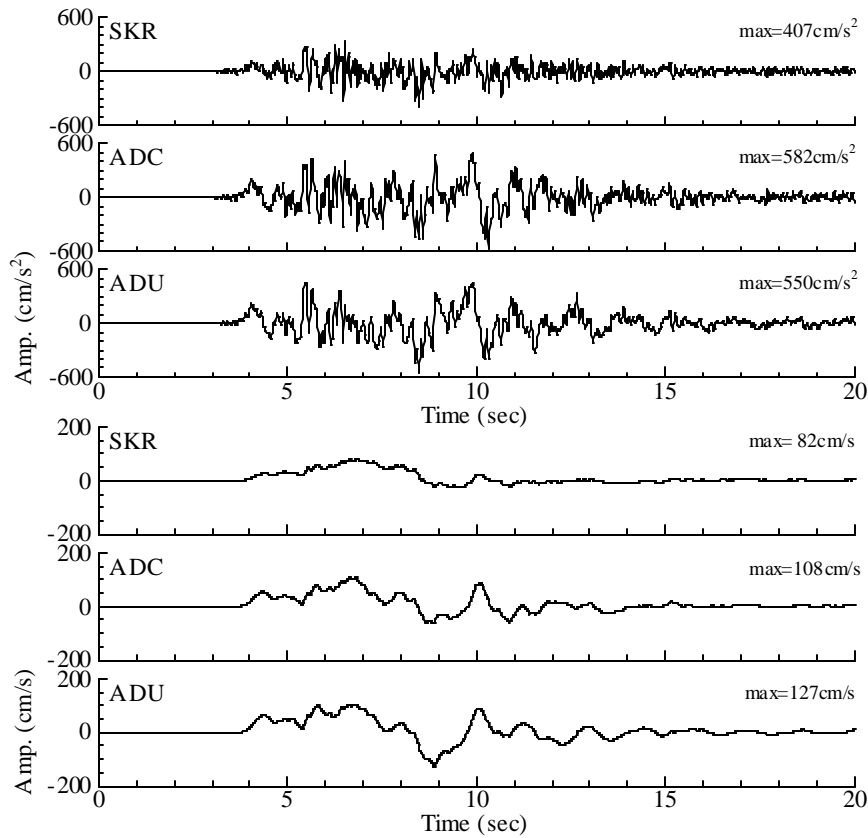


Figure 15.　　　Observed ground accelerations and integrated velocities during the mainshock without any filtering processes at SKR and synthetic ground motions at ADC and ADU, assuming 1D propagation of S-wave without any corrections of distance and non-linearity.
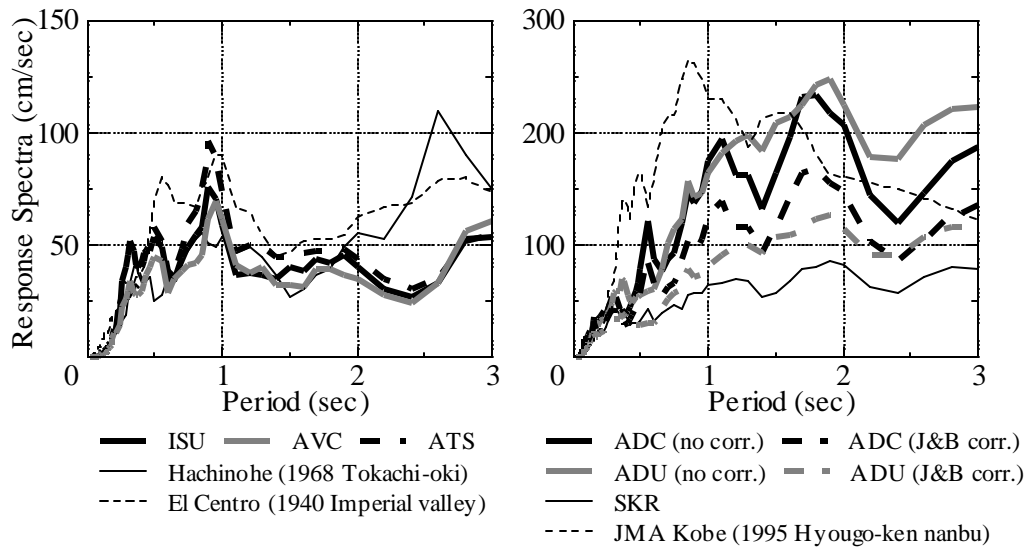
Figure 16.    Comparison of the pseudo velocity response spectra (h=5 %) of the simulated and the observed strong motions during the mainshock with those of strong motion records that have been used in earthquake engineering. Estimated ground motion at Avcilar (AVC, ISU) during the mainshock is similar to those at Hachinohe and El Centro as shown in the left figure. The thick solid and broken lines in the right figure indicate the response spectra at ADC without distance correction and with the correction using the empirical relationship by Joyner and Boore (1983), respectively. Similarly, the gray solid and broken lines also indicate those at ADU with and without distance correction, respectively.